

Effect of Fiber Optic Chromatic Dispersion on the Performance of Analog Optical Link with External Modulation Aiming at Aerospace Applications

Antonio Alves Ferreira Júnior¹, Olympio Lucchini Coutinho², Carla de Sousa Martins³, William dos Santos Fegadoli², José Antônio Justino Ribeiro¹, Vilson Rosa de Almeida⁴, José Edimar Barbosa Oliveira²

ABSTRACT: This paper addresses the subject of fiber optic chromatic dispersion effect on the performance of analog optical link with dual-drive electro-optic Mach-Zehnder modulator, aiming at aerospace applications. Thus, a direct detection link model that emphasizes both the modulator electronic drive and the dispersion characteristic of a linear optical fiber is discussed. Furthermore, a mathematical approach yielding a rather insightful analysis of the link performance for either optical double or single sideband modulation formats is fully discussed. It is worthwhile to point out that such modeling has the special feature of relying on a uniform nomenclature, which enables one to quickly retrieve a wide range of known results regarding optical fiber link performance that are already available on an ample literature. The model usefulness is illustrated by predicting the performance dependence of a direct detection fiber optic link with respect to the radiofrequency and link length. Results of numerical simulations for a link that comprises commercial optoelectronic components with potential for practical application on electronic warfare field were also provided.

KEYWORDS: Dual-drive Mach-Zehnder modulator, Analog fiber optic link, Fiber optic chromatic dispersion, Optical single sideband modulation, Optical double sideband modulation.

INTRODUCTION

Due to the increasing evidence that radio-over-fiber technology will be playing a major role in global interconnectivity, many efforts have been directed toward researches and development on the field of fiber optic link. A great deal of emphasis continues to be driven by important military and commercial demands, which aim at previously unachievable performance on the subjects of radiofrequency (RF) and microwave signal processing, radio-over-fiber, and antenna-remoting (Yao, 2012a, 2012b). Nowadays, analog photonic links have attracted significant interest in many applications, such as phased array antennas, radar systems, broadband cable-television (CATV) networks, ROF access wireless communications, and so on (Capmany *et al.*, 2013; Yao, 2012c; Zhang *et al.*, 2012a, 2012b; Wu *et al.*, 2011).

Aiming at aerospace applications, the remote radar antenna could be placed at a distance of several kilometers from the central office, and the generated radar signals could be distributed to other antennas for tracking an aircraft, or to other central offices (Oliveira *et al.*, 1999; Coutinho *et al.*, 2011; Lim *et al.*, 2009). This versatility is very interesting because human resources and equipments can be allocated in a safety and controlled place, while the remote radar antenna is

¹.Instituto Nacional de Telecomunicações – Santa Rita do Sapucaí/MG – Brazil ².Instituto Tecnológico de Aeronáutica – São José dos Campos/SP – Brazil ³.Instituto de Pesquisas da Marinha – Rio de Janeiro/RJ – Brazil ⁴.Instituto de Estudos Avançados – São José dos Campos/SP – Brazil

Author for correspondence: Antonio Alves Ferreira Júnior | Instituto Nacional de Telecomunicações | Avenida João de Camargo, 510 | CEP 37.540.000 Santa Rita do Sapucaí/MG – Brazil | E-mail: antonioa@inatel.br

Received: 20/11/12 | Accepted: 09/04/13

located at field, as suggested in Fig. 1a. A central office that is connected to a large number of base stations via optical fiber may be used in a high capacity metropolitan optical fiber network to distribute data signals from various communications systems to users or to another optical fiber network area, as illustrated in Fig. 1b (Yao, 2012b; Lim *et al.*, 2010).

At the input end of such links, an optical laser diode generates a carrier at a desired optical wavelength, and a dual-drive electro-optic Mach-Zehnder modulator (DD-MZM) imposes an analog RF signal (e.g. radar signal) on the optical carrier. This signal is applied to an optical fiber link, whereas at the output end of the link a photodetector (PD) is employed to recover the analog RF signal from its optical carrier, and then processed by a RF front-end and delivered to a load (e.g. remote radar antenna). It is worthwhile to point out that the DD-MZM plays an important role in the link for it enables the wideband implementation of either optical

single sideband (OSSB) or optical double sideband (ODSB) modulation formats.

This publication is concerned with the effect of fiber optic chromatic dispersion on the performance of links that operate based on external intensity modulation and direct detection techniques, called IM/DD optical links configuration. Assuming a balanced 50/50 splitting ratio of the DD-MZM Y-junctions, a rigorous analysis of the chromatic dispersion effect on the performance of the analog link was provided by Corral *et al.* (2001). However, the expressions are in the form of infinite series. Such drawback is overcome in Cheng *et al.* (2005), where an analytical model, in which the modulation indexes of the two DD-MZM drives can be unbalanced, yields a closed-form expression for the power at the output of the detector. Nevertheless, fabrication tolerances make a balanced DD-MZM particularly difficult to achieve, hence practical modulators have a finite extinction rate. Therefore, a general model that allows the study of all these cases will be very helpful for the system design.

STATEMENT OF THE PROBLEM

A typical schematic representation of the IM/DD link with a transmitter, an optical channel, and a receiver is illustrated in Fig. 2a. In Fig. 2b an external electro-optic modulator electronic driver is emphasized.

At the input of the fiber optic link, a continuous wave from a distributed feedback single-mode laser diode (DFB-LD) generates an optical carrier at a desired wavelength/frequency with a complex optical field given by Yariv and Yeh (2007), as seen in Eq. 1:

$$E_o(t) = \sqrt{2\xi P_o(t)} e^{j[\omega_o t + \phi_o]} \tag{1}$$

where ω_o is the mean optical frequency, ϕ_o is an arbitrary initial optical phase, $P_o(t)$ is the optical power, and ξ (ohms per square meter) is a constant that depends on both the laser beam effective cross-section and the optical wave impedance.

The present publication relies on the often used approach in the analysis of IM/DD optical links according to which the laser average power and its phase are time invariant (Corral *et al.*, 2001; Cheng *et al.*, 2005).

In Fig. 2b one should notice that the optical power delivered by the laser diode reaches the input Y-junction of the integrated z-cut LiNbO₃ DD-MZM, and then it is divided into two parcels according to a splitting ratio, determined

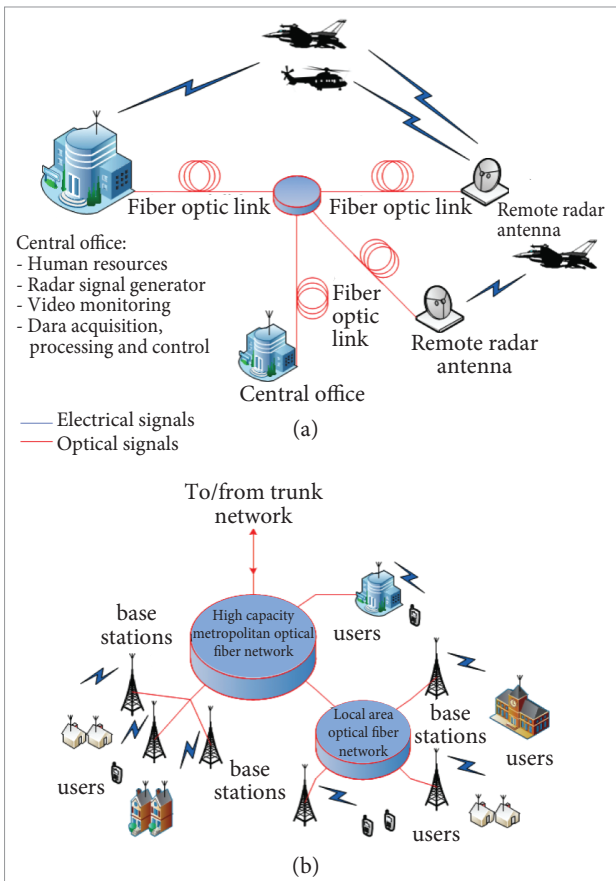


Figure 1. Fiber optic links (a) connecting a central office and the remote radar antenna aiming at aerospace applications, and (b) for data system communications.

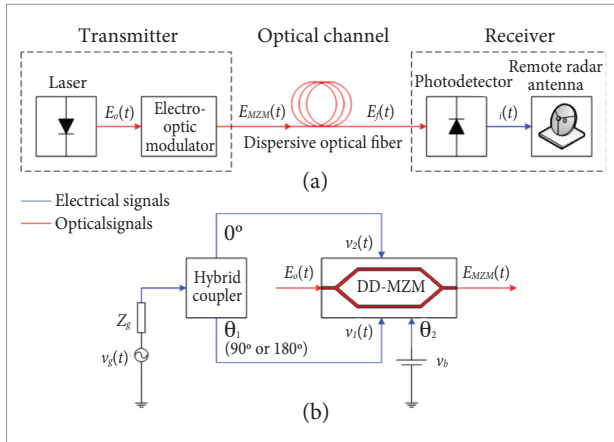


Figure 2. Overall architecture of the IM/DD analog fiber optic link, where (a) shows the transmitter, optical channel and receiver, and (b) presents the external electro-optic modulator with the electronic driver.

by the Y-junction power transmission coefficient r_1 (Lin *et al.*, 2008). The simplified view of an integrated DD-MZM is illustrated in Fig. 3 (Morant *et al.*, 2011; Janner *et al.*, 2008), where (A) shows the top view in which the optical waveguides are properly positioned with respect to the RF modulation field pattern, and (B) presents the cross-section view.

Once a MZM's configuration is specified, as shown in Fig. 3, its performance dependence on substrate orientation and geometry of electrodes can be predicted through the variation of the optical phase factor. Using a standard perturbation analysis, such variation turns into Eq. 2 (Kitano and Oliveira, 2000):

$$\Delta\beta_{op}^{TE, TM} = \frac{\omega_o^2 \mu \epsilon_0}{2\beta_{op}^{TE, TM}} \frac{\int_{-\infty}^{+\infty} \int_{-\infty}^{+\infty} \bar{E}_{TE, TM}^*(x, z) \cdot [-\epsilon_{ii} \epsilon_{jj} r_{ijk} E_k^{(m)}(x, z)] \bar{E}_{TE, TM}(x, z) dx dz}{\int_{-\infty}^{+\infty} \int_{-\infty}^{+\infty} \bar{E}_{TE, TM}^*(x, z) \cdot \bar{E}_{TE, TM}(x, z) dx dz} \quad (2)$$

where $\beta_{op}^{TE, TM}$ and $E_{TE, TM}$ are the unperturbed optical phase factor and electric field for TE or TM modes, respectively; $E_k^{(m)}$ is the RF modulation electric field; r_{ijk} and ϵ_{ii} are the components of the electro-optic tensor and electric permittivity of LiNbO₃, respectively. Equation 2 shows that as a consequence of the electro-optic effect, a RF signal can be used to control the phase of the optical field associated with each optical power parcels as they propagate through the

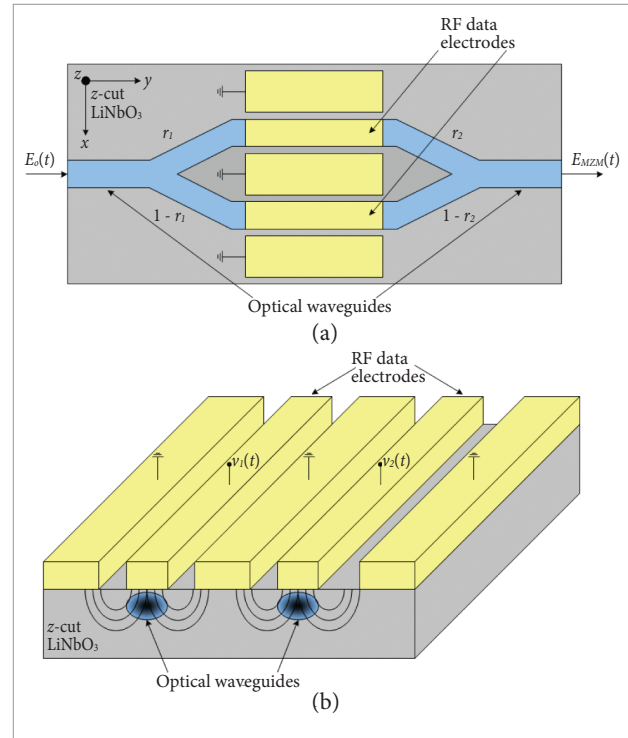


Figure 3. Simplified integrated dual-drive electro-optic Mach-Zehnder modulator (DD-MZM) scheme with a z-cut LiNbO₃ substrate using an optical transverse magnetic (TM) mode, where (a) is the top view showing transmission coefficients of the Y-junctions, and (b) demonstrates the cross-section view.

distinct arms of the DD-MZM. It is worthwhile to point out that in the configuration selected in Fig. 3 the optical guided mode has TM polarization, since it enables the use of the strongest LiNbO₃ electro-optic coefficient, namely r_{33} .

The RF signal, henceforth named modulation signal, must generate an electric field with both a temporal and a spatial pattern adequately distributed in order to reach some key performance requirements, such as low RF power consumption and wide RF bandwidth (Kitano and Oliveira, 2000; Oliveira and Ribeiro, 2000). A great deal of such control may be achieved through the drive electronics, by properly choosing the phase shift (θ_1) and the bias (θ_2) of the electrical signal applied to the modulator electrodes, as indicated in Fig. 2b. According to Fig. 2, the instantaneous values of the modulating signals applied to the lower and upper electrodes of MZM, are as in Eqs. 3a and 3b:

$$v_1(t) = V_1 \cos(\omega_{RF} t + \theta_1) \quad (3a)$$

$$v_2(t) = V_2 \cos(\omega_{RF} t) \quad (3b)$$

where V_1 and V_2 are the amplitudes of signals in the lower and upper arms, ω_{RF} is the angular frequency of the RF signal, and θ_1 is the phase difference between the signals. The optical phase variations introduced in the arms of the modulator through linear electro-optic effect are given by Eq. 4:

$$\phi_1(t) = \frac{\pi}{V_\pi} v_1(t) = m_1 \cos(\omega_{RF}t + \theta_1) \tag{4a}$$

$$v_2(t) = V_2 \cos(\omega_{RF}t) \tag{4b}$$

$$\phi_b(t) = \frac{\pi}{V_\pi} V_b = \theta_2 \tag{4c}$$

where V_π is the MZM half-wave switching voltage that can be calculated using Eq. 2, and θ_2 is the phase variation due to the voltage bias applied to the proper access. The coefficients m_1 and m_2 are the modulation indexes due to their signals in the lower and upper arms, which are given, respectively, by Eqs. 5a and 5b:

$$m_1 = \frac{\pi V_1}{V_\pi} \tag{5a}$$

$$m_2 = \frac{\pi V_2}{V_\pi} \tag{5b}$$

Based on the schematic representation illustrated in Fig. 3a and taking into account the splitting ratio of the output Y-junction r_2 , it can be shown that the optical electrical field at the output of the DD-MZM has a complex form given by Eq. 6:

$$E_{MZM}(t) = E_o e^{j\omega_o t} \left\{ \sqrt{r_1 r_2} e^{j[m_1 \cos(\omega_{RF}t + \theta_1) + \theta_2]} + \sqrt{(1-r_1)(1-r_2)} e^{j m_2 \cos(\omega_{RF}t)} \right\} \tag{6}$$

where $E_o = \sqrt{(2\xi P_o)}$.

It should be pointed out that Eq. 6 applies to DD-MZM with both arbitrary splitting ratio and modulation signals. Such general situation often occurs in the real world, either at the fabrication stage of the modulator or in field applications. The optical signal at the output of the modulator

with electric field given by Eq. 6 feeds a spool of standard single-mode optical fiber (SSMF) with a step-index profile, circular dielectric waveguide and length L , as illustrated in Fig. 4a. This simplified representation has n_1 and n_2 as the refractive indexes of the core and cladding with radius a and b , respectively (Yariv and Yeh, 2007). As an example, typical values of core and cladding diameters of a commercial fiber is 8.2 and 125 μm , respectively (Corning®, 2002).

For instance, in the fiber modeling, a fused silica glass SSMF operating at 1,550 nm wavelength is considered to be linear with constant loss $\alpha(\omega)$ (dB per kilometer), whereas the phase factor $\beta(\omega)$ (radians per meter) exhibits dependence with respect to the frequency deviation and chromatic dispersion. The optical field signal is affected by the attenuation and the phase factors after propagates through an optical fiber with length L , as shown in Fig. 4a. In order to achieve different values for the chromatic dispersion parameter, optical fibers with index profiles as illustrated in Fig. 4b are often used to this purpose, like the nonzero-dispersion shifted (NZ-DSF) and the zero-dispersion shifted (DSF) (Agrawal, 2002; Li and Nolan, 2008).

In the model of fiber optic propagation characteristics, one should bear in mind the presence of three phenomena in the fiber channel, which are different in nature, occur

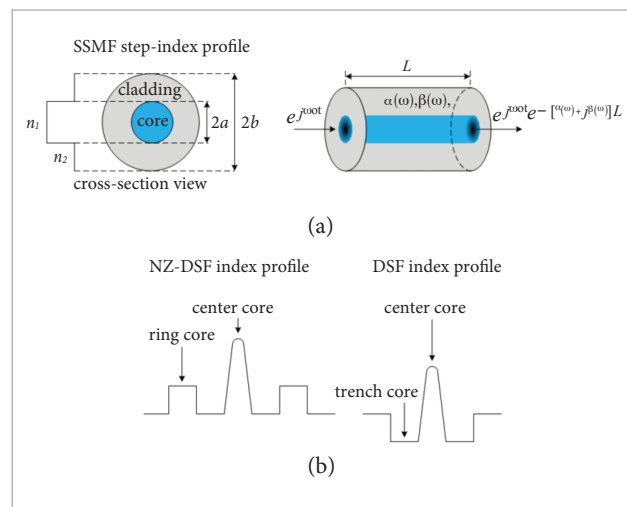


Figure 4. (a) A simplified representation of a step-index profile standard single-mode optical fiber (SSMF) with circular dielectric waveguide, and the optical signal affected by the attenuation and phase factors after being propagated through an optical fiber with length L ; (b) Index profiles often used to nonzero-dispersion shifted (NZ-DSF) and the zero-dispersion shifted (DSF) optical fibers.

simultaneously, and influence each other, namely: noise, filtering, and Kerr nonlinearity (Essiambre *et al.*, 2010). This publication is mainly concerned with the filtering phenomenon that stems from the chromatic dispersion of the fiber, including waveguide and material (Winzer and Essiambre, 2006). In order to understand these characteristics, for a SSMF we will use the Fig. 5 with the results that were published in Essiambre *et al.* (2010) and Li and Nolan (2008).

Regarding SSMF attenuation, as see in Fig. 5a (Essiambre *et al.*, 2010), the 1,550 nm transmission window has the lowest attenuation value, around 0.2 dB/km, compared with the 1,310 nm transmission one, which is around 0.35 dB/km. However, the SSMF chromatic dispersion value, red line in Fig. 5b (Li and Nolan, 2008), at 1,550 nm is around 17 ps/nm.km, while the 1,310 nm has zero-dispersion. The green and purple lines refer to NZ-DSF and DSF, respectively, where some types of index profiles for these fibers were presented in Fig. 4b.

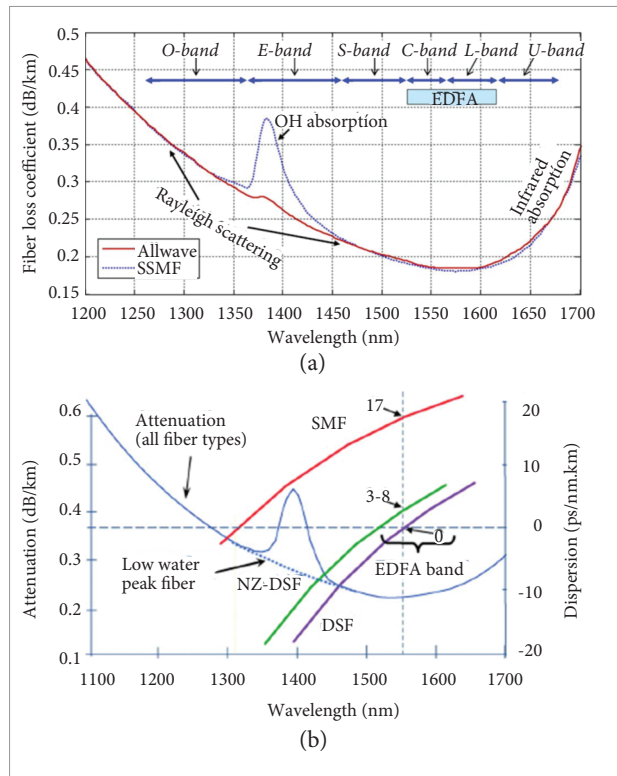


Figure 5. Spectral dependence of fiber optic characteristics, where (a) is the behavior of attenuation factor (Essiambre *et al.*, 2010), and (b) is its chromatic dispersion parameter for three types of fiber: standard single-mode optical fiber – SSMF (red), nonzero-dispersion shifted – NZ-DSF (green) and the zero-dispersion shifted – DSF (purple) (Li and Nolan, 2008).

The 1,550 nm window (C-band) is widely used for long-haul transmission system and the advance in research of erbium-doped fibers amplifiers (EDFA) made possible the use of this device in wavelength-division multiplexing (WDM) systems. However, the DSF were not suitable for WDM, because the nonlinear effect of four-wave mixing (FWM) is the strongest when the dispersion is zero. Certain amount of dispersion is desirable to reduce the FWM effect, being the NZ-DSF proposed. Some techniques to design optical fibers have been developed to achieve a desired value for the chromatic dispersion parameter (Li and Nolan, 2008). All the optical signal spectral components will propagate through the fiber optic with different velocities, and the phase of each component will be changed by chromatic dispersion. Bearing in mind that an exact functional form is rarely known, its expansion in Taylor series around the carrier frequency ω_0 as Agrawal (2002) performed is useful (Eq. 7):

$$\beta(\omega) = \beta_0(\omega_0) + \beta_1(\omega_0)(\omega - \omega_0) + \frac{1}{2}\beta_2(\omega_0)(\omega - \omega_0)^2 + \frac{1}{6}\beta_3(\omega_0)(\omega - \omega_0)^3 + \dots \quad (7)$$

The high order terms were not considered. The four ones on the right side shows distinct dependence about the frequency deviation. The first term is constant and related to phase velocity of optical carrier, the second varies linearly, and $\beta_1(\omega_0)$ determines the group velocity that is related to the group delay. The third has a quadratic dependence and it is related to the derivative of group velocity with respect to the frequency. The interesting here is on $\beta_2(\omega_0)$ coefficient related to the fiber chromatic dispersion parameter $D(\lambda)$, the optical carrier wavelength (λ_0), and the speed of light (c) in vacuum, according to Eq. 8 (Agrawal, 2002):

$$\beta_2(\omega_0) = -\frac{D(\lambda)\lambda_0^2}{2\pi c} \quad (8)$$

While the phase factor $\beta(\omega)$ presents dependence with respect to the frequency, the chromatic dispersion parameter $D(\lambda)$ has it with optical wavelength and can be modeled by a Taylor's series expansion around the operation wavelength (Wandel and Kristensen, 2006). However, a practical insightful expression can be seen as in Eq. 9 (Corning[®], 2002):

$$D(\lambda) = \frac{S_0}{4} \left(\lambda - \frac{\lambda_0^4}{\lambda^3} \right) \quad (9)$$

where S_0 is the zero-dispersion slope and a typical value is less than 0.092 ps/nm².km (Corning®, 2002), λ is the operation wavelength (nm), and λ_0 is the zero-dispersion wavelength (nm). The $\beta_3(\omega_0)$ parameter in Eq. 7 can be obtained from the high order derivatives of phase factor, or it is defined as the derivative of $\beta_2(\omega_0)$ with respect to the frequency. It contributes to the calculation of the dispersion slope $S(\lambda)$, which has dependence with optical wavelength, as Eq. 10 (Winzer and Essiambre, 2006):

$$S(\lambda) = \frac{d}{d\lambda} [D(\lambda)] = \left(\frac{4\pi c}{\lambda^3} \right) \beta_2 + \left(\frac{2\pi c}{\lambda^2} \right)^2 \beta_3 \quad (10)$$

At the output end of the SSMF, a square law PD transforms the photon stream into a RF electric current. When introducing the concept of PD responsivity, it can be shown that the electrical photocurrent is proportional to the incident average optical power, hence it is also to the magnitude of the optical Poynting vector. Assuming a uniform power distribution over the fiber cross section, the time dependent RF current is as in Eq. 11:

$$i(t) = \Re \frac{E_f(t)E_f^*(t)}{2\xi} + n(t) \quad (11)$$

where \Re is the PD responsivity, ξ (ohms per square meter) is a constant that depends on both the fiber effective cross-section and the optical wave impedance, and $E_f(t)$ is the optical electrical field at the fiber link output according to Fig. 2a. The $n(t)$ accounts for PD additive noises sources, such as thermal and shot noises (Lim *et al.*, 2009; Yariv and Yeh, 2007). However, the noise subject will not be addressed in this publication.

As will be shown later, Eq. 11 reveals that by applying the fiber output to the PD, beating signals between the optical spectral components will generate harmonics of the original RF modulating signal. The characteristics of these depend on both the fiber optic chromatic dispersion and the modulation format, which will be used to estimate the performance of the link.

OPTICAL FIBER LINK MODEL

As previously stated, the present study is concerned with links based on DD-MZM having a 50/50 splitting ratio. Hence, using Eq. 6, the output electrical field in the complex form turns out to be expressed as Eq. 12:

$$E_{MZM}(t) = \frac{E_o}{2} e^{j\omega_o t} \left[\sum_{n=-\infty}^{+\infty} j^n J_n(m_1) e^{jn(\omega_{RF}t + \theta_1)} e^{j\theta_2} + \sum_{n=-\infty}^{+\infty} j^n J_n(m_2) e^{jn\omega_{RF}t} \right] \quad (12)$$

where $J_n(\cdot)$ represents the first kind Bessel's function with order n . By rewriting Eq. 12 in Eqs. 13 and 14:

$$E_{MZM}(t) = \frac{E_o}{2} e^{j\omega_o t} \sum_{n=-\infty}^{+\infty} a_n e^{jn\omega_{RF}t} \quad (13)$$

$$a_n = j^n [J_n(m_1) e^{j(n\theta_1 + \theta_2)} + J_n(m_2)] \quad (14)$$

It is readily seen that the optical field at the DD-MZM output indeed consists of an infinite series of optical spectral components, i.e. an optical carrier component at ω_0 and an infinite number of sidebands, with frequencies $\omega = \omega_0 \pm n\omega_{RF}$ and amplitude a_n . A small-signal analysis was performed in Ferreira Júnior *et al.* (2012), which enables one to identify the requirement that should be satisfied by the DD-MZM drive electronics in order to provide certain modulation formats. For example, single sideband (OSSB), double sideband (ODSB), and carrier suppressed (OCS) optical modulation formats can be obtained when the pair of parameters (θ_1, θ_2) obeys the following constraint: $(\pi/2, \pm\pi/2)$, $(\pi, \pm\pi/2)$, and (π, π) , respectively.

In order to further develop the analysis of the link, one should analyze again Eq. 13. Taking into account the linear nature of the fiber optic and bearing in mind the spectral composition of the optical field at the output of the DD-MZM, we tackled the effect of the chromatic dispersion with the help of Eq. 7. Thus, we have obtained the following expression for the phase factor of an optical spectral component with frequency equal to $\omega = \omega_0 \pm n\omega_{RF}$ (Eq. 15):

$$\beta(\omega_0 \pm n\omega_{RF}) = \beta_0(\omega_0) \pm \beta_1(\omega_0) n\omega_{RF} + \frac{1}{2} \beta_2(\omega_0) (n\omega_{RF})^2 \pm \frac{1}{6} \beta_3(\omega_0) (n\omega_{RF})^3 + \dots \quad (15)$$

Using this result in combination with Maxwell's equations, we undertook the time domain analysis of the propagation of the optical field given by Eq. 13 along a linear SSMF. The expression obtained for the output electrical field after propagation through a fiber with length L is given by Eq. 16:

$$E_f(t) = 10^{-\frac{\alpha_{dB}L}{20}} \frac{E_o}{2} e^{j\omega_o t} \sum_{n=-\infty}^{+\infty} a_n e^{jn\omega_{RF}t} e^{j\frac{1}{2}(n\omega_{RF})^2 \beta_2(\omega_o)L} \quad (16)$$

Once more, we remember the linear characteristics of the fiber optics under consideration. Therefore, it might be possible to benefit from standard techniques developed for frequency domain analysis of system. First, we took the Fourier's transform of Eq. 16 from a linear system, and after some mathematical manipulations, we obtained Eq. 17 for the electrical field in the frequency domain:

$$E_f(\omega) = 10^{-\frac{\alpha_{dB}L}{20}} \pi E_o \sum_{n=-\infty}^{+\infty} a_n \delta(\omega - n\omega_{RF}) e^{j\frac{1}{2}(n\omega_{RF})^2 \beta_2(\omega_o)L} \quad (17)$$

where δ represents the Dirac's delta function. Therefore, we must be able to use the model to predict dependence on frequency of such current. To this aim, we first remember that the convolution theorem can be applied to rewrite the time domain expression of the PD current, as given by Eq. 11 in the frequency domain, as Eq. 18:

$$I(\omega) = \Re \frac{E_f(\omega) * E_f^*(\omega)}{4\pi\xi} \quad (18)$$

where the mathematical symbol * denotes convolution. Then, Eqs. 19, 20 and 21 were obtained for the RF current Fourier's transform, under the condition $n=N+k$:

$$I(\omega) = 2\pi \sum_{N=-\infty}^{+\infty} I(N\omega_{RF}) \delta(\omega - N\omega_{RF}) \quad (19)$$

$$I(N\omega_{RF}) = 10^{-\frac{\alpha_{dB}L}{10}} \frac{\Re P_o}{4} e^{j\frac{N\phi}{2}} \sum_{k=-\infty}^{+\infty} a_{N+k} a_k^* e^{jk\phi} \quad (20)$$

$$\phi = N\omega_{RF}^2 \beta_2(\omega_o)L \quad (21)$$

Equation 19 was achieved without introducing any approximation and is in perfect agreement with results published by many authors (Corral *et al.*, 2001; Cheng *et al.*, 2005). Until a few years ago, using such formulas to predict the

spectral components of the PD current was rather cumbersome and yielded little physical insight, except when one assumed a small signal approximation. It is worth to remember such complexity mostly stems from the fact that the coefficient $a_{N+k} a_k^*$ involves the product of Bessel's function, as it is readily seen in Eq. 14.

However, a few years ago such drawback was overcome through the application of Graf's addition theorem for Bessel's functions (Cheng *et al.*, 2005; Chi and Yao, 2008). In order to be able to take advantage of such theorem in the analysis presented in this publication, we have used Eq. 14 to calculate $a_{N+k} a_k^*$ and then substituted the obtained result into Eq. 20. After some mathematical manipulations we obtained expressions for $I(N\omega_{RF})$ and for the detected DC current ($N=0$), which besides allowing the retrieving of previous results, it also includes a few parameters such as the fiber attenuation, PD responsivity and laser output power. These were not explicitly accounted for in previous publications. Such expressions are given, respectively, by Eqs. 22 and 23:

$$I(N\omega_{RF}) = 10^{-\frac{\alpha_{dB}L}{10}} \frac{\Re P_o}{4} \cdot \left\{ e^{jN\left(\theta_1 + \frac{\phi + \pi}{2}\right)} \sum_{k=-\infty}^{+\infty} J_{N+k}(m_1) J_k(m_1) e^{jk\phi} + e^{jN\left(\frac{\phi + \pi}{2}\right)} \sum_{k=-\infty}^{+\infty} J_{N+k}(m_2) J_k(m_2) e^{jk\phi} + e^{j\left[N\left(\theta_1 + \frac{\phi + \pi}{2}\right) + \theta_2\right]} \sum_{k=-\infty}^{+\infty} J_{N+k}(m_1) J_k(m_2) e^{jk(\phi + \theta_1)} + e^{j\left[N\left(\frac{\phi + \pi}{2}\right) - \theta_2\right]} \sum_{k=-\infty}^{+\infty} J_{N+k}(m_2) J_k(m_1) e^{jk(\phi - \theta_1)} \right\} \quad (22)$$

$$I(0) = 10^{-\frac{\alpha_{dB}L}{10}} \frac{\Re P_o}{4} \sum_{k=-\infty}^{+\infty} \left[J_k^2(m_1) + J_k^2(m_2) + 2J_k(m_1) J_k(m_2) \cos(k\theta_1 + \theta_2) \right] \quad (23)$$

Furthermore, Eqs. 6 and 22 enable to quickly retrieve previous results with DD-MZM having infinite extinction ratio ($r_1 = r_2 = 0.5$), and when the modulation indexes are equal ($m_1 = m_2 = m$). Since the intention was to compare our predictions with previous publications, Graf's addition

theorem was applied for Bessel's functions (Abramowitz and Stegun, 1965) to Eq. 22, under the assumption that the modulation indexes are equal, resulting in Eq. 24:

$$I(N\omega_{RF}) = 10^{\frac{-\alpha_{dB}L}{10}} \frac{\Re P_o}{4} \cdot \left\{ \begin{aligned} & \left[e^{jN(\theta_1+\pi)} + e^{jN\pi} \right] J_N \left[2m \sin\left(\frac{\phi}{2}\right) \right] + \\ & + e^{j \left[N\left(\frac{\theta_1}{2}+\pi\right) + \theta_2 \right]} J_N \left[2m \sin\left(\frac{\phi+\theta_1}{2}\right) \right] + \\ & + e^{j \left[N\left(\frac{\theta_1}{2}+\pi\right) - \theta_2 \right]} J_N \left[2m \sin\left(\frac{\phi-\theta_1}{2}\right) \right] \end{aligned} \right\} \quad (24)$$

In this publication, the modeling of the analog fiber optic link is synthesized by Eq. 24. It enables the frequency domain analysis of how the fiber optic chromatic dispersion affects the link performance which employ DD-MZM.

The ϕ parameter, which is given in Eq. 21, takes into account the harmonic order, RF, chromatic dispersion, and fiber optic length. The optical modulation format can be specified by properly selecting the parameters θ_1 and θ_2 . This article follows the approach adopted in Cheng *et al.* (2005), and the two situations addressed are obtained when either $\theta_1 = \pi$ (ODSB) or $\theta_1 = \pi/2$ (OSSB), with $\theta_2 = \pi/2$ for both cases.

Usually, the performance of the fiber link is evaluated in terms of the RF power delivered to output load (R_L), and the average power of the harmonic with order N is (Eq. 25):

$$P_{R_L}(N\omega_{RF}) = \frac{1}{2} |I(N\omega_{RF})|^2 R_L \quad (25)$$

In order to compare the exact analytical model, Eqs. 24 and 25, with a particular case of small-signal approximation ($m \ll 1$), which is widely discussed in the literature (Lim *et al.*, 2010), the detected RF fundamental ($N = 1$) power is (Eq. 26):

$$P_{R_L}(\omega_{RF}) = \left(\frac{10^{\frac{-\alpha_{dB}L}{5}} m^2 P_o^2 \Re^2 R_L}{8} \right) \cos^2 \left(\frac{\pi L D f_{RF}^2 \lambda_o^2}{c} \right) \quad (26)$$

Impedance matching networks are often used at the DD-MZM input and PD output to provide the maximum signal power transfer, due to the frequency response of these

devices. In this work, all the impedances were considered purely resistive and matched. In Eq. 26, the modulation index (m) is related to signal power (P_{RF}) and impedance (Z_g) of the RF source, and to the DD-MZM input impedance (Z_{MZM}). The RF power delivered to the load (P_{RL}) is related to the PD output impedance (Coutinho *et al.*, 2005).

NUMERICAL RESULTS AND DISCUSSION

The numerical simulations were developed by using commercial components with parameters specified in Table 1. To validate our model, first of all we developed our simulations with exactly the same link parameters used in Cheng *et al.* (2005) and they were presented in Ferreira Júnior *et al.* (2012).

Figure 6a shows the normalized RF fundamental power for 10 GHz frequency in function of fiber optic length, for both exact and small-signal approximations, using the ODSB modulation: $(\theta_1, \theta_2) = (\pi, \pi/2)$. It is observed that the results are in perfect agreement and the modeling presented can recover previous simulations (Lim *et al.*, 2010). However, if the modulation index increases, i.e. large-signal condition, the small-signal approximation moves away from the exact analysis as shown in Fig. 6b. It can be seen that the increases in a RF power do not improve the performance of the link.

In order to observe the fiber optic length (L) in which the RF power is minimum, this periodic variation, under the condition

Table 1. Typical values of parameters used in the simulation

Parameter description	Symbol	Value
RF source impedance	Z_g	50 Ω
RF load impedance	Z_L	50 Ω
RF power applied to DD-MZM	P_{RF}	1 mW
Laser optical power	P_o	1 mW
Laser wavelength	λ_o	1,550 nm
DD-MZM half-wave voltage	V_π	5 V
DD-MZM input impedance	Z_{MZM}	50 Ω
SSMF fiber attenuation @ 1,550 nm (Corning [®] , 2002)	α_{dB}	0.2 dB/km
SSMF fiber chromatic dispersion @ 1,550 nm (Corning [®] , 2002)	D	17 ps/nm.km
Speed of light in vacuum	c	3x10 ⁸ m/s
PD responsivity	\Re	0.5 A/W

RF: radiofrequency; DD-MZM: dual-drive electro-optic Mach-Zehnder modulator; SSMF: standard single-mode optical fiber; PD: photodetector.

with low and equal modulation indexes ($m_1 = m_2 = m \ll 1$) and fundamental RF frequency ($N = 1$), can be predicted by Eq. 27:

$$L_p = \frac{(2p + 1)c}{2Df_{RF}^2 \lambda_o^2} \quad (27)$$

where $p = 0, 1, 2$, etc. The dispersion effect exhibits a cyclic behavior and the period length is determined by Eq. 28:

$$\Delta L = \frac{c}{Df_{RF}^2 \lambda_o^2} \quad (28)$$

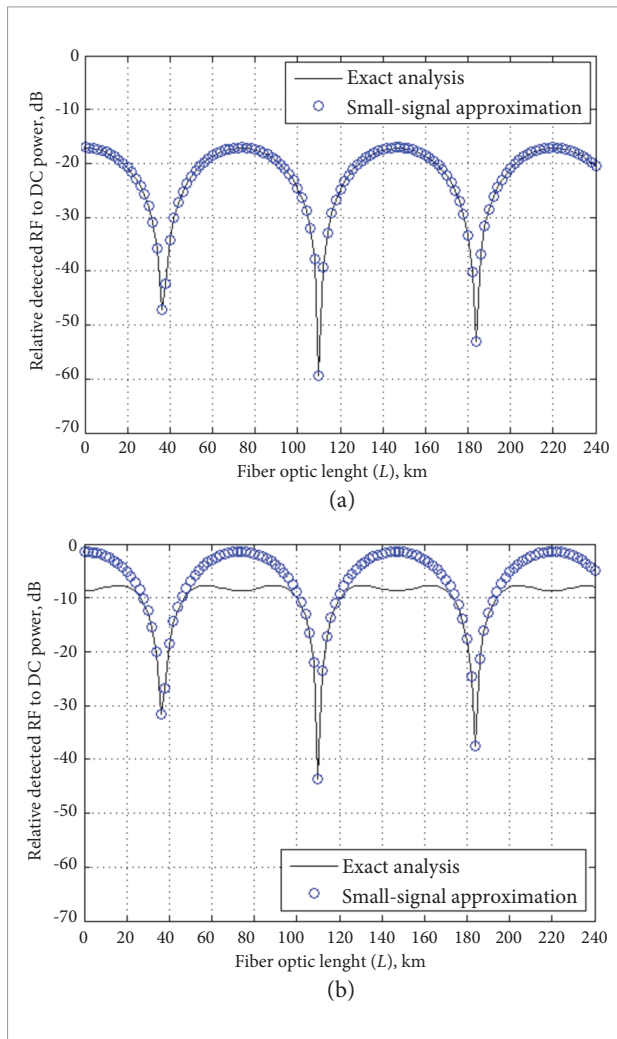


Figure 6. Detected radiofrequency (RF) fundamental ($N = 1$) power normalized to the direct current (DC) level versus fiber length, for exact and small-signal approximations, under conditions: (a) small- ($m = 0.2$), and (b) large-signals ($m = 1.2$). The RF is equal to 10 GHz and uses optical double sideband (ODSB) modulation $(\theta_1, \theta_2) = (\pi, \pi/2)$.

Similar results were presented considering only the first minimum point (Gliese *et al.*, 1996). The influence of chirp effect in the fiber length in which the RF power is minimum was observed in Smith *et al.* (1997).

Based on Eqs. 6 and 22, the authors have been investigating the chirp modeling of DD-MZM as a function of both the splitting ratio and modulation indexes, and the results will be published elsewhere. For instance, the relative detected RF fundamental power to DC level versus RF, with fiber optic length (L) equals 40 km, for ODSB push-pull ($m_1 = m_2 = m$, $\theta_1 = \pi$, $\theta_2 = \pi/2$), single-arm ($m_2 = 0$, $\theta_1 = \pi$, $\theta_2 = +\pi/2$ and $-\pi/2$), and OSSB ($m_1 = m_2 = m$, $\theta_1 = \pi/2$, $\theta_2 = \pi/2$) modulations are presented in Fig. 7.

It is observed in Fig. 7 that the analytical formulation presented in this paper is in agreement with experimental results obtained by Han *et al.* (2003), which the expressions are in infinite series form. For a single-arm ODSB modulation, the frequency that the detected power is minimized could be changed by adjusting the bias parameter θ_2 . The dependence of the fundamental RF power for the ODSB modulation is strongly affected by the chromatic dispersion and the power is minimized in approximately 10 GHz. This is the so-called notch filter like behavior. For OSSB modulation, the link exhibits the special feature of RF fundamental power displaying very low sensitivity with respect to both the fiber length and the RF. Such unique feature has been

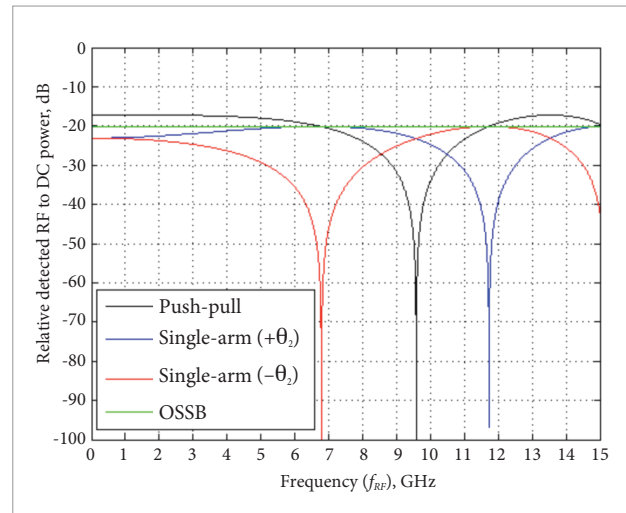


Figure 7. Detected fundamental radiofrequency – RF ($N = 1$) power normalized to the direct current (DC) level versus frequency for optical double sideband (ODSB) push-pull and single-arm, and optical single sideband (OSSB) modulations, with $\theta_2 = \pi/2$, $L = 40$ km.

widely exploited in practical applications on the subject of microwave photonics, as in aerospace and long-haul fiber optical telecommunications (Urlick *et al.*, 2011).

It is important to point out that the principle of energy conservation is obeyed, i.e. in this analysis the fundamental RF power ($N = 1$) is minimized in a specific RF for the ODSB modulation $(\theta_1, \theta_2) = (\pi, \pi/2)$, according to Fig. 7. The energy is transferred to the harmonics of superior orders ($N = 2, 3, \dots$) and DC level ($N = 0$). The summation of RF power of all spectral components is the same for each value of RF (or fiber optic length). Figure 8 shows the detected RF power *versus* RF for $N = 0, 1, 2$, with fiber optic length (L) equals to 40 km.

In order to be able to better illustrate the effect of the chromatic dispersion in the RF fundamental ($N = 1$) power, it is convenient to analyze its dependence with respect to the length of the fiber. To this aim we first tackled the ODSB modulation $(\theta_1, \theta_2) = (\pi, \pi/2)$, and the results are shown in Fig. 9. As can be seen, irrespective of the RF, the chromatic dispersion results in a periodic variation of the RF power as the fiber length increases. The position along the fiber at which the RF power is minimized depends on the RF. For example, when the RF is 20 GHz, the first minimum occurs at approximately 10 km, whereas for a 10 GHz frequency this is nearly 36 km. Using Eqs. 27 and 28 allows one to calculate the fiber length in which the RF power is minimum.

CONCLUSION

This publication presented a very comprehensive analytical model that enables the analysis of the effect of fiber optic chromatic dispersion in the performance of analog fiber optic link with DD-MZM. The model besides relying on parameters that suits experimental researchers, also allows one to retrieve important results widely available in the literature. Using some commercial components and devices, we performed numerical simulations that yielded results, which seem to be of practical interest. The authors are working towards designing, implementing, and characterizing fiber link based on the model developed.

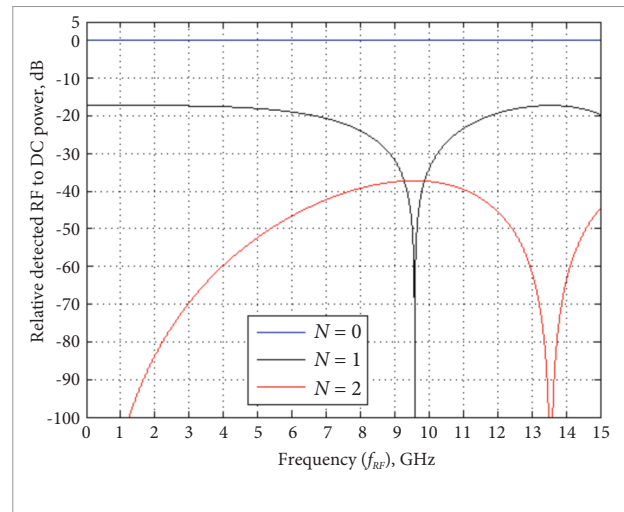


Figure 8. Detected radiofrequency (RF) power normalized to the direct current (DC) level *versus* frequency, with $N = 0$ (DC), $N = 1$ (fundamental) and $N = 2$ (second harmonic), for optical double sideband (ODSB) modulation $(\theta_1, \theta_2) = (\pi, \pi/2)$ with $L = 40$ km.

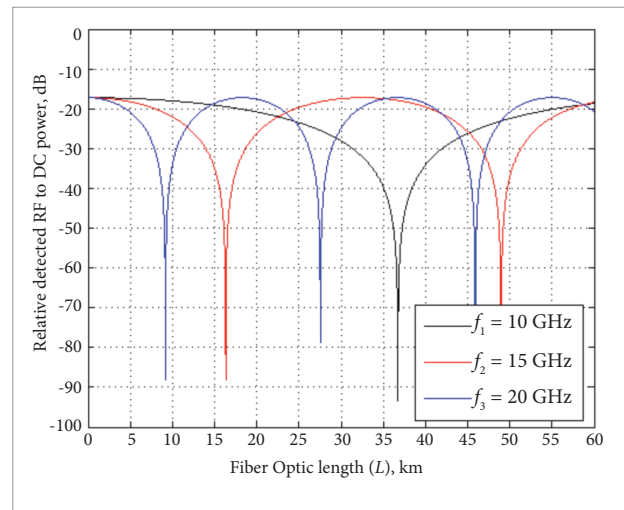


Figure 9. Detected radiofrequency (RF) fundamental [$N = 1$] power normalized to the direct current (DC) level *versus* fiber optic length, with RF as a parameter for optical double sideband (ODSB) modulation $(\theta_1, \theta_2) = (\pi, \pi/2)$.

ACKNOWLEDGMENTS

To the Electronic Warfare Laboratory at the Instituto Tecnológico de Aeronáutica (ITA) and the Instituto Nacional de Telecomunicações (INATEL) for their support in this research.

REFERENCES

- Abramowitz, M. and Stegun, I., 1965, "Handbook of Mathematical Functions with Formulas, Graphs, and Mathematical Tables", Dover Publications, New York.
- Agrawal, G.P., 2002, "Fiber-Optic Communication Systems", 3rd edition, John Wiley & Sons, New York.
- Capmany, J. *et al.*, 2013, "Microwave Photonic Signal Processing", *Journal of Lightwave Technology*, Vol. 31, No. 4, pp. 571-586. doi:10.1109/JLT.2012.2222348.
- Cheng, L. *et al.*, 2005, "An Exact Analytical Model for Dispersive Transmission in Microwave Fiber-Optic Links Using Mach-Zehnder External Modulator", *IEEE Photonics Technology Letters*, Vol. 17, No. 7, pp. 1525-1527. doi:10.1109/LPT.2005.848563.
- Chi, H. and Yao, J., 2008, "Power Distribution of Phase-Modulated Microwave Signals in a Dispersive Fiber-Optic Link", *IEEE Photonics Technology Letters*, Vol. 20, No. 4, pp. 315-317. doi:10.1109/LPT.2007.915653.
- Corning®, 2002, "SMF-28™ Optical Fiber Product Information". Retrieved in April 29, 2013, from <http://www.photonics.byu.edu/FiberOpticConnectors.parts/images/smf28.pdf>.
- Corral, J.L. *et al.*, 2001, "General expressions for IM/DD dispersive analog optical links with external modulation or optical up-conversion in Mach-Zehnder electrooptical modulator", *IEEE Transactions on Microwave Theory and Techniques*, Vol. 49, No. 10, pp. 1968-1976. doi:10.1109/22.954816.
- Coutinho, O.L. *et al.*, 2005, "Analysis of analog fiber optical links based on DSB+C and SSB+C modulation techniques", In: *International Conference on Microwave and Optoelectronics – SBMO/IEEE MTT-S*, pp. 439-443. doi:10.1109/IMOC.2005.1580038.
- Coutinho, O.L. *et al.*, 2011, "Uso de redes de comunicações ópticas para transmissão e distribuição de emissores radar", In: *Simpósio de Aplicações Operacionais em Áreas de Defesa – XIII SIGE*, São José dos Campos, SP, Brazil.
- Essiambre, R.J. *et al.*, 2010, "Capacity limits of optical fiber networks", *Journal of Lightwave Technology*, Vol. 28, No. 4, pp. 662-701. doi:10.1109/JLT.2009.2039464.
- Ferreira Júnior, A.A. *et al.*, 2012, "Effect of fiber optic chromatic dispersion on the performance of analog optical link with dual-drive Mach-Zehnder modulator", In: *Simpósio de Aplicações Operacionais em Área de Defesa – XIV SIGE*, pp. 119-126, São José dos Campos, SP, Brazil.
- Gliese, U. *et al.*, 1996, "Chromatic dispersion in fiber-optic microwave and millimeter-wave links", *IEEE Transactions on Microwave Theory and Techniques*, Vol. 44, No. 10, pp. 1716-1724. doi:10.1109/22.538964.
- Han, J. *et al.*, 2003, "Reduction of fiber chromatic dispersion effects in fiber-wireless and photonic time-stretching system using polymer modulators", *Journal of Lightwave Technology*, Vol. 21, No. 6, pp. 1504-1509. doi:10.1109/JLT.2003.812155.
- Janner, D. *et al.*, 2008, "Waveguide electro-optic modulation in micro-engineered LiNbO₃", *Journal of Optics A*, No. 10, pp. 01-06. doi:10.1088/1464-4258/10/10/104003.
- Kitano, C. and Oliveira, J.E.B., 2000, "Dispositivos à Óptica Integrada para Aplicações em Telecomunicações", *Revista Telecomunicações*, Vol. 3, No. 2, pp. 27-38.
- Li, M.J. and Nolan, D.A., 2008, "Optical Transmission Fiber Design Evolution", *Journal of Lightwave Technology*, Vol. 26, No. 9, pp. 1079-1092. doi:10.1109/JLT.2008.922150.
- Lim, C. *et al.*, 2010, "Fiber-Wireless Networks and Subsystem Technologies", *Journal of Lightwave Technology*, Vol. 28, No. 4, pp. 390-405. doi:10.1109/JLT.2009.2031423.
- Lim, W. *et al.*, 2009, "Analytical time-domain model for radio over free space optical military communication systems under turbulence channels", In: *IEEE Military Communications Conference – MILCOM 2009*, Paper 901734, pp. 1-5. doi:10.1109/MILCOM.2009.5379930.
- Lin, C. *et al.*, 2008, "Impact of nonlinear transfer function and imperfect ratio of MZM on optical up-conversion employing double sideband with carrier suppression modulation", *Journal of Lightwave Technology*, Vol. 26, No. 15, pp. 2449-2459. doi:10.1109/JLT.2008.927160.
- Morant, M. *et al.*, 2011, "Dual-drive LiNbO₃ interferometric Mach-Zehnder architecture with extended linear regime for high peak-to-average OFDM-based communication systems", *Optics Express*, Vol. 19, No. 26, pp. 450-456. doi:10.1364/OE.19.008452.
- Oliveira, J.E.B. *et al.*, 1999, "Trends in photonics applied to electronic warfare at Brazilian airforce", In: *International Microwave and Optoelectronics Conference – SBMO/IEEE MTT-S*, pp. 599-602, Rio de Janeiro, RJ, Brazil. doi:10.1109/IMOC.1999.866252.
- Oliveira, J.E.B. and Ribeiro, J.A.J., 2000, "Interfaces para enlaces de fibra óptica de alta velocidade", *Revista Telecomunicações*, Vol. 3, No. 2, pp. 65-75.
- Smith, G.H. *et al.*, 1997, "Overcoming Chromatic-Dispersion Effects in Fiber-Wireless Systems Incorporating External Modulators", *IEEE Transactions on Microwave Theory and Techniques*, Vol. 45, No. 8, pp. 1410-1415. doi:10.1109/22.618444.
- Urick, V.J. *et al.*, 2011, "Long-Haul Analog Photonics", *Journal of Lightwave Technology*, Vol. 29, No. 8, pp. 1182-1205. doi:10.1109/JLT.2011.2119292.
- Wandel, M. and Kristensen, P., 2006, "Fiber designs for high figure of merit and high slope dispersion compensating fibers", *Journal of Optical and Fiber Communications Research*, Vol. 3, No. 1, pp. 25-60. doi:10.1007/s10297-005-0061-1.
- Winzer, P.J. and Essiambre, R.J., 2006, "Advanced Optical Modulation Formats", *Proceedings of the IEEE*, Vol. 94, No. 5, pp. 952-985. doi:10.1109/JPROC.2006.873438.
- Wu, P.Y. *et al.*, 2011, "An upconverted phase-modulated fiber optical CATV transport system", *Journal of Lightwave Technology*, Vol. 29, No. 16, pp. 2422-2427. doi:10.1109/JLT.2011.2160330.
- Yao, J., 2012a, "A tutorial on microwave photonics I", *IEEE Photonics Society Newsletter*, Vol. 26, No. 2, pp. 4-12.
- Yao, J., 2012b, "A tutorial on microwave photonics II", *IEEE Photonics Society Newsletter*, Vol. 26, No. 3, pp. 5-12.



Yao, J., 2012c, "Microwave Photonics," In: IEEE International Workshop on Electromagnetics, Applications and Student Innovation – iWEM, pp. 1-2. doi:10.1109/iWEM.2012.6320333.

Yariv, A. and Yeh, P., 2007, "Photonics: Optical Electronics in Modern Communications", 6th edition, Oxford University Press, New York.

Zhang, H. *et al.*, 2012a, "Polarization-modulated analog photonic

link with compensation of the dispersion-induced power fading", Optics Letters, Vol. 37, No. 5, pp. 866-868. doi:10.1364/OL.37.000866.

Zhang, G. *et al.*, 2012b, "Postcompensation for nonlinearity of Mach-Zehnder modulator in radio-over-fiber system based on second-order optical sideband processing", Optics Letters, Vol. 37, No. 5, pp. 806-808. doi:10.1364/OL.37.000806.